Optical and magneto-optical properties and giant magnetoresistance of Fe/Cr superlattices with noncollinear alignment of iron layers

V. V. Ustinov, M. M. Kirillova, I. D. Lobov, V. M. Maevskii, A. A. Makhnev, V. I. Minin, L. N. Romashev, A. R. Del', A. V. Semerikov, and E. I. Shreder

Institute of Metal Physics, Urals Division of Russian Academy of Sciences, 621019 Ekaterinburg, Russia
(Submitted 10 March 1995, after revision 26 June 1995)
Zh. Éksp. Teor. Fiz. **109**, 477–494 (February 1996)

A study of optical and magneto-optical properties and of giant magnetoresistance of Fe/Cr superlattices is reported. Two independent approaches to the determination of the misalignment angle between magnetizations of neighboring iron layers based on measurements of the equatorial Kerr effect and of magnetoresistance are proposed. Experimental data are interpreted in terms of the theory of odd magneto-optical effects assuming that interfaces between layers are sharp, and a theory of alignment effects on magnetoresistance using the model of biquadratic exchange is developed. We conclude that there is a noncollinear magnetic ordering in Fe/Cr superlattices with the initial misalignment angle being a function of the chromium thickness. © *1996 American Institute of Physics.* [S1063-7761(96)01202-6]

1. INTRODUCTION

Metal superlattices are a new class of materials with unusual physical properties. In some superlattices, such as Co/Pt and Co/Pd,[1–3] the Kerr rotation in the ultraviolet band is considerably larger than in pure cobalt, hence they are promising for magneto-optical storage of data. Another important feature of magnetic multilayered structures is the giant magnetoresistive effect, which was first discovered in the Fe/Cr/Fe three-layered structure.[4] Experiments with Fe/Cr superlattices[5] demonstrated that the giant magnetoresistive effect, which is about 10% at the room temperature and about 50% at 4.2 K, is due to the antiferromagnetic ordering of Fe layers, hence due to the indirect exchange between Fe layers. Later[6–8] the researchers found out that the energy of exchange antiferromagnetic coupling is a damped oscillating function of the chromium layer thickness d_{Cr}, which decays with d_{Cr} and has the first maximum at 9 Å and the second maximum at 27 Å . The oscillations of the exchange energy have been discussed in terms of the generalized Ruderman–Kittel–Kasui–Yosida theory.[9–11]

The indirect exchange in magnetic superlattices has drawn considerable attention to studies of magnetic ordering in these structures. The magnetic ordering in Fe/Cr films was detected in experiments on polarization of scattered neutrons and in measurements of hysteresis loops using the Kerr rotation.[12–16] Ferro- and antiferromagnetic ordering, as well as the 90°-ordering were detected in magneto-optical measurements of hysteresis loops in the Fe/Cr/Fe system.[16] In the Si(111)/Cr(100Å){Fe(32Å)/Cr(10Å)}$_{20}$/Cr(10Å) structure[12] the angle between magnetizations of neighboring iron layers is close to 180° at ~1 kOe and 90° at 4 kOe. A noncollinear magnetic structure with a misalignment angle between magnetic moments of neighboring iron layers $\theta = 50°$ was discovered in the {Fe(53Å)/Cr(17Å)}$_9$ structure.[17]

The study of the magnetic ordering pattern, including possible cases of noncollinear ordering, is an important step in understanding the nature of magnetic interaction in superlattices and distinctive features of their magnetic characteristics. In the reported work our aim was to estimate the misalignment angles between magnetizations of iron layers in Fe/Cr superlattices both in the initial state and in an external magnetic field. We used two approaches to achieve this aim. The first one is based on measurements of frequency, angular, and field dependences of the equatorial Kerr effect, and analysis of data in terms of the theory of magneto-optic effects in multilayered structures. The second approach is based on studies of magnetic-alignment effects on the superlattice magnetoresistance and on processing the data using the concept of the biquadratic exchange and formation of noncollinear magnetic ordering. The objects studied were Fe/Cr superlattices with typical thicknesses of chromium layers d_{Cr} for which the magnetic ordering is close to the antiferromagnetic state.[6]

We have also studied optical properties of superlattices depending on the dielectric response of a layered metallic structure in the band in which spectra of the equatorial Kerr effect were recorded.

2. SAMPLES AND EXPERIMENTAL TECHNIQUES

The structures containing {Fe(23 Å)/Cr(8 Å)}$_{30}$ (1), {Fe(20 Å)/Cr(11 Å)}$_{30}$ (2), and {Fe(23 Å)/Cr(27 Å)}$_{12}$ (3) superlattices were fabricated by the molecular beam epitaxy in the Katun'-S facility. Starting materials with a purity of 99.9% were placed in previously baked zirconium oxide crucibles. Mass spectra of the chamber atmosphere with hot crucibles (without evaporated metals) did not show traces of any materials except the usual residual gases. Metal layers were grown on magnesium oxide substrates, whose lattice parameters are best matched to those of Fe/Cr superlattices. Substrates with the (100) orientation were etched chemically and baked in vacuum at 10^{-8} Pa and 600 °C. A buffer ~120-Å chromium layer was grown on each substrate. The substrate temperature during the growth was maintained at 160–240 °C. The vacuum in the growth chamber was 10^{-6}–10^{-7} Pa. The thicknesses of the iron and chromium layers were derived from the growth rate and time.[18]

 1063-7761/96/020253-09$10.00

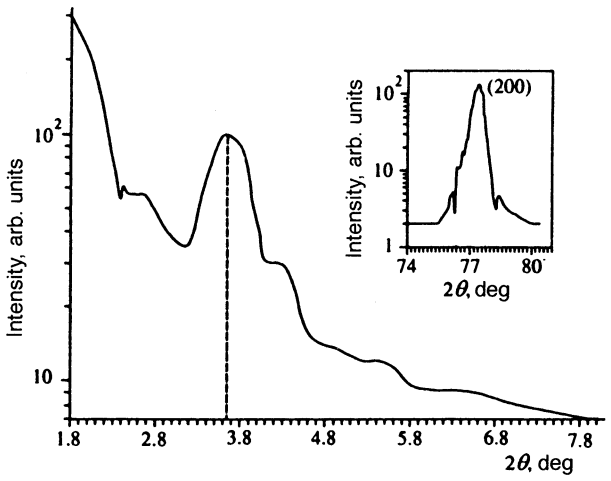

FIG. 1. Intensity of X-rays diffracted from the {Fe(20Å)/Cr(11Å)}$_{30}$/Cr(140 Å)/MgO structure versus angle in the range of small angles. The insert shows the (200) Bragg reflection due to Fe and Cr layers.

The crystal structure of the fabricated films was monitored in-process by the diffraction pattern recorded by a built-in HEED diffractometer. Then the crystal structure was analyzed by a DRON-3M X-ray diffractometer. Diffraction patterns were recorded using the K_α(Co) line in the two-crystal configuration, and the monochromator was a Si(111) plate. In high-angle (2θ) X-ray diffraction patterns of {Fe/Cr }MgO(100) superlattices, a peak corresponding to Fe(200) and Cr(200) reflections was recorded. In the range of small angles, a peak due to the superstructure was detected in all samples (Fig. 1). The diffraction patterns indicated that the superlattices grown on MgO(100) substrates were single crystals. The coherence length derived from X-ray diffraction data was 180–200 Å for all superlattices.

The effective complex dielectric function $\varepsilon_{\text{eff}}=\varepsilon'_{\text{eff}} - i\varepsilon''_{\text{eff}}$ was measured by the Beattie ellipsometric technique at a light incidence angle $\varphi=75°$ in the spectral band $\lambda=0.25$–2.5 μm. The equatorial Kerr effect (δ_p-effect) was measured in the spectral band 0.27–2.4 μm on a computerized magneto-optical spectrometer.[19] Curves of the δ_p-effect versus angle were recorded at wavelengths of 0.27, 0.6, and 2.4 μm, and versus field at 0.6 μm.

The magnetoresistance parameters were measured by the traditional four-terminal technique in a magnetic field ranging from 0 to 23 kOe aligned either with planes of superlattice layers or with the normal to the sample surface.

3. OPTICAL AND MAGNETO-OPTICAL PROPERTIES OF SUPERLATTICES

3.1. Optical properties

Like a stack of plates, a superlattice is an optically anisotropic structure with the axis perpendicular to its layers.[20] Since all metals in the visible and IR bands have $|\varepsilon|\gg 1$, the optical anisotropy in ellipsometric measurements of light reflected from its basis plane is very small (the differences are of order $1/|\varepsilon|$).

Curves of the effective optical conductivity $\sigma_{\text{eff}}=\omega\varepsilon''_{\text{eff}}/4\pi$, where ω is the circular light frequency, versus

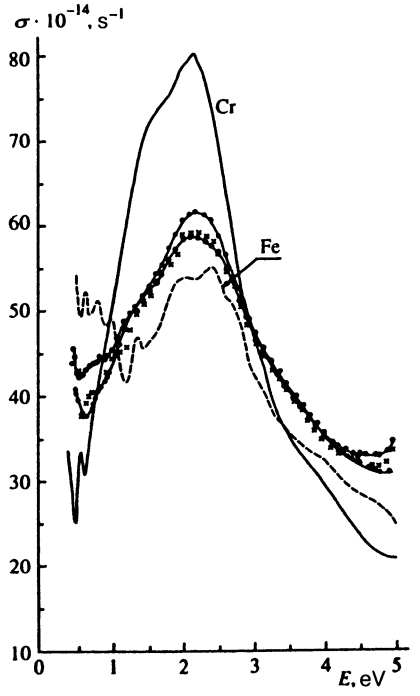

FIG. 2. Effective optical conductivity σ_{eff}: ○) {Fe(23 Å)/Cr(8 Å)}$_{30}$; ×) {Fe(20 Å)/Cr(11 Å)}$_{30}$; ●) {Fe(23 Å)/Cr(27 Å)}$_{12}$. Optical conductivity of single crystals of Fe [Ref. 22] (dashed line) and Cr [Ref. 21] (solid line).

the photon energy for superlattices, pure iron and chromium are given in Fig. 2. There is an intense absorption band[21] centered at 2.2 eV in chromium, and its intensity and position are independent of its magnetic ordering. An absorption band in this range of photon energies is also present in the iron spectrum.[22] According to calculations of its energy bands, it is largely due to electron transitions between bands with spin down (↓). Experimental data indicate that this band is also not sensitive to the iron magnetic ordering.[23]

One can see in Fig. 2 that the curves of the optical conductivity of the superlattices also have an absorption band typical of these metals, lying between those of iron and chromium almost throughout the spectral band studied. The analysis of these data based on the formula for σ_{eff}[24] revealed that the superlattice dielectric response can be approximated as a weighted average of the dielectric responses of pure metals and indicated that the individual optical properties of Fe and Cr in thin layers are presesued. An important point is that the high optical conductivity σ_{eff} is an additional confirmation of the good structural quality of the samples.

3.2. Theory of equatorial Kerr effects in a multilayered structure

Let us consider a model multilayered structure composed of plane parallel uniformly magnetized layers shown in Fig. 3a. Optical parameters of all materials ($j=1,2,\ldots,N$ is the layer index) are assumed to be isotropic. The outside medium ($j=1$), from which the light is incident at an angle φ, is totally transparent. All other materials may be absorbing. The widths of the layers, d_j, and magnetization directions in the layers are arbitrary. Each material is characterized by a dielectric $\hat{\varepsilon}_j$ and a permeability $\hat{\mu}_j$ ten-

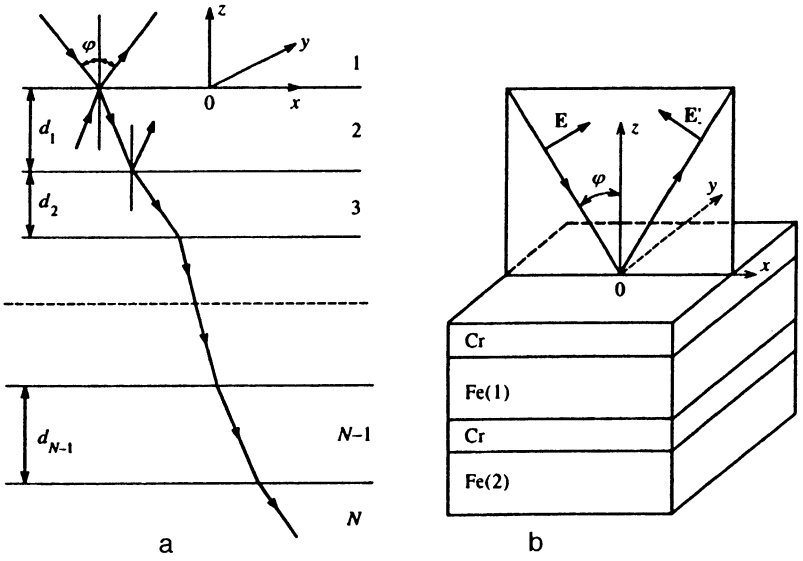

FIG. 3. a) Diagram of light beams in a multilayered structure in a general case; b) diagram of measurement of the equatorial Kerr effect in a Fe/Cr superlattice: E, E′ are the electric-field intensities of the incident and reflected waves, φ is the angle of incidence, xy is the surface plane.

sors, which are described in the optical range and in the approximation linear in the magnetization by the formula

$$\hat{\varepsilon}_j = n_j^2 \begin{pmatrix} 1 & 0 & iQ_p^{(j)} \\ 0 & 1 & 0 \\ -iQ_p^{(j)} & 0 & 1 \end{pmatrix};$$

$$\hat{\mu}_j = \begin{pmatrix} 1 & 0 & iQ_s^{(j)} \\ 0 & 1 & 0 \\ -iQ_s^{(j)} & 0 & 1 \end{pmatrix}, \tag{1}$$

where i is the imaginary unit, n_j is the refraction index of the material, and $Q_p^{(j)}$ and $Q_s^{(j)}$ are the magneto-optical parameters ($|Q_{p(s)}^{(j)}| \ll 1$) proportional to the saturation magnetization. In a nonmagnetic material $Q_p^{(j)} = Q_s^{(j)} = 0$.

Let us determine the reflection factors of p-polarized (in the light incidence plane) and s-polarized (perpendicular to the incidence plane) light waves on interfaces between layers. The reflection factors on the interface between the j-th and k-th layer are described by Fresnel's formulas

$$r_{jk}^s = \frac{g_j - g_k}{g_j + g_k}, \quad r_{jk}^p = \frac{g_j n_k^2 - g_k n_j^2}{g_j n_k^2 + g_k n_j^2}, \tag{2}$$

where

$$g_j = g_j' - i g_j'' = \sqrt{n_j^2 - n_1^2 \sin^2 \varphi}, \quad g_j', g_j'' \geqslant 0. \tag{3}$$

Let us determine the reflectivity of a multilayered structure (without regard for the magnetization of the layers) using the Heavens matrix technique.[25] Let $j, j+1, \ldots, m$ be an increasing set of layer indices ($j = 1,2,\ldots,N-1$, $m = 2,3,\ldots,N$) of a multilayered structure. The two-dimensional Heavens' matrix for this structure is[25]

$$B = \prod_{k=j}^{m-1} \begin{pmatrix} 1 & F_k^2 r_{k,k+1} \\ r_{k,k+1} & F_{k+1}^2 \end{pmatrix} = \begin{pmatrix} B_{11} & B_{12} \\ B_{21} & B_{22} \end{pmatrix}, \tag{4}$$

where $r_{k,k+1}$ are the reflection factors defined by Eq. (2) (indices s and p are omitted), and the phase factors

$$F_k = \exp\left(-2\pi i \frac{g_k d_k}{\lambda}\right) \tag{5}$$

are functions of the phase increments of light (λ is its wavelength in vacuum) and its absorption in a layer with a thickness d_k. By definition, $F_m = 1$. Order of the layer indices is reversed ($j, j-1, \ldots, m$), the following matrix is generated:

$$B = \prod_{k=j}^{m+1} \begin{pmatrix} 1 & F_{k-1}^2 r_{k,k-1} \\ r_{k,k-1} & F_{k-1}^2 \end{pmatrix} = \begin{pmatrix} B_{11} & B_{12} \\ B_{21} & B_{22} \end{pmatrix}, \tag{6}$$

where we have $F_m = 1$ by definition. Then in structures with the increasing ($j < m$) or decreasing ($j > m$) order of indices, the reflection factors of forward (propagating along the z-axis) and backward (propagating in the opposite direction) waves are determined by the formulas (the overline denotes backward waves)

$$r(B) = \frac{B_{21}}{B_{11}}, \quad \bar{r}(B) = \frac{B_{12}}{B_{22}}. \tag{7}$$

If a p- or s-polarized wave is incident on a multilayered structure (Fig. 3a), the effects of magnetization on the intensity of reflected (into layer 1) or transmitted (into layer N) light are odd in the magnetization and are called equatorial Kerr effects. The amplitude of the equatorial Kerr effect, $\delta = (I - I_0)/I_0$, where I and I_0 are the intensities of light in the nonmagnetized and magnetized states, respectively, is described by the formulas[26] (indices r and t refer to reflected and transmitted light, respectively):

$$\delta_{s(p)}^{(r)} = 2\,\mathrm{Re} \sum_{j=2}^{N} R_{s(p)}^{(j)} A_{s(p)}^{(j)}, \quad \delta_{s(p)}^{(t)} = 2\,\mathrm{Re} \sum_{j=2}^{N} T_{s(p)}^{(j)} A_{s(p)}^{(j)}, \tag{8}$$

where

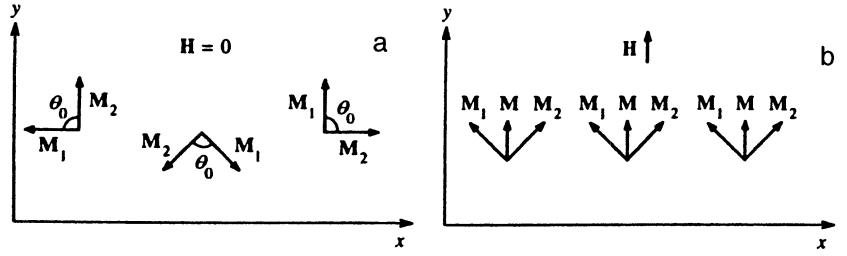

FIG. 4. Diagrams of Fe/Cr(100) superlattice magnetization in the equatorial field. The magnetizations of iron layers, $\mathbf{M}_1$ and $\mathbf{M}_2$, and the external field $\mathbf{H}$ are aligned with the surface plane, $\mathbf{M}=(\mathbf{M}_1+\mathbf{M}_2)/2$.

$$A_{s(p)}^{(j)}=i(1-F_j^2)\frac{n_1 Q_{s(p)}^{(j)}}{2g_j}\sin\varphi\cos\gamma_j,$$

$$T_{s(p)}^{(j)}=\frac{r_{j\ldots2,1}^{s(p)}-r_{j\ldots N-1,N}^{s(p)}}{1-F_j^2 r_{j\ldots2,1}^{s(p)} r_{j\ldots N-1,N}^{s(p)}}, \tag{9}$$

$$R_{s(p)}^{(j)}=T_{s(p)}^{(j)}-\frac{1-\bar{r}_{j\ldots2,1}^{s(p)} r_{j\ldots N-1,N}^{s(p)}}{\bar{r}_{j\ldots2,1}^{s(p)}-F_j^2 r_{j\ldots N-1,N}^{s(p)}}.$$

In Eq. (9), n_1 is the ambient refraction factor, φ is the light incidence angle, g_j is the parameter defined in Eq. (3), γ_j is the angle between the magnetization vector and the y-axis in the j-th layer (equatorial angle), and the reflection factors $r_{j\ldots2,1}^{s(p)}$, $\bar{r}_{j\ldots2,1}^{s(p)}$, and $r_{j\ldots N-1,N}^{s(p)}$ are determined by Eq. (7).

Note some features of the equatorial Kerr effects deriving from Eqs. (8) and (9). These effects are controlled only by the equatorial magnetization components (along the normal y to the plane of incidence of the light). When the incident light is s-polarized, the equatorial Kerr effect is caused by the off-diagonal component $\mu_{xz}^{(j)}=iQ_s^{(j)}$ of the permeability tensor (gyromagnetic effects), and if the light is p-polarized, it is due to the component $\varepsilon_{xz}^{(j)}=i\varepsilon_j Q_p^{(j)}$ (gyroelectric effects). The following proportionality relation can be derived:

$$R_{s(p)}^{(j)}\propto(F_2F_3\ldots F_{j-1})^2\cos\varphi, \tag{10}$$

from which it follows with due account of Eqs. (3) and (5) that in structures with absorbing layers the factors $R_{s(p)}^{(j)}$ for magnetized layers at a depth larger than the skin thickness tend to zero, and the contribution of these layers to the equatorial Kerr effect is also vanishing. It follows from Eqs. (9) and (10) that the equatorial Kerr effect on reflected light is always zero at angles of incidence $\varphi=0°$ and 90°. Note also that the sum in Eq. (8) is in effect taken only over magnetized layers because in nonmagnetized layers $A_{s(p)}^{(j)}=0$.

4. MANIFESTATION OF EXCHANGE COUPLING BETWEEN IRON LAYERS IN THE EQUATORIAL KERR EFFECT

The configuration of the equatorial Kerr effect measurements using light reflected from a Fe/Cr superlattice ($\delta_p^{(r)}$-effect) is shown in Fig. 3b. An alternating magnetizing field is aligned perpendicularly to the plane of incidence of the light (parellel to the y-axis), and the incident wave is polarized in the plane of incidence (p-polarization). The experimental data were compared to calculations of the $\delta_p^{(r)}$-effect by Eqs. (8) and (9). The calculation used the widths of the chromium and iron layers (d_{Cr} and d_{Fe}) given in Sec. 2 and the optical constants and Q_p of iron derived from measurements of thick (about 1000 Å) films of iron and chromium.[18]

Our interpretation of the magneto-optical measurements is based on the concept of magnetic ordering in the Fe/Cr superlattice due to the exchange coupling between neighboring iron layers separated by a chromium spacer.[6–8] We assume that in the general case the exchange coupling in zero magnetic field gives rise to noncollinear ordering of the ferromagnetic layers, i.e., the magnetization vectors $\mathbf{M}_1$ and $\mathbf{M}_2$ of neighboring layers are turned through an angle θ_0 with respect to each other. The angle θ_0 ranges from 0 (ferromagnetic ordering) to 180° (antiferromagnetic ordering) and is a basic characteristics of the superlattice magnetic structure. The Fe/Cr(100) superlattices studied in our experiments are easily magnetized in-plane,[27] when the external magnetic field $\mathbf{H}$ is aligned with the sample plane and magnetization vectors $\mathbf{M}_1$ and $\mathbf{M}_2$ are in the same plane with an angle $\theta(H)$ between them. We presume that in structures with iron layers of equal thickness $|\mathbf{M}_1|=|\mathbf{M}_2|$ holds the angles and θ_1 and θ_2 between the vectors $\mathbf{M}_1$ and $\mathbf{M}_2$, and the average magnetization $\mathbf{M}=(\mathbf{M}_1+\mathbf{M}_2)/2$ aligned with the external magnetic field $\mathbf{H}$ are equal: $\theta_1=\theta_2=\theta/2$. We also assume that the exchange energy exceeds the magnetic anisotropy energy. Thus we have the following model of superlattice magnetization with noncollinear magnetic ordering. When the external magnetic field is zero, the superlattice is separated into domains, the magnetization vectors $\mathbf{M}_1$ and $\mathbf{M}_2$ of two neighboring layers being aligned with the layer plane (xy-plane) and the angle between them equal in all the domains, $\theta=\theta_0$. This configuration is shown schematically in Fig. 4a. This pattern is translated in the vertical direction to other pairs of iron layers. An external magnetic field $\mathbf{H}=(0,H,0)$ causes all average magnetization vectors $\mathbf{M}=(\mathbf{M}_1+\mathbf{M}_2)/2$ to be aligned with the external field (Fig. 4b). If the external field is much smaller than the saturation field H_s, the angle θ_0 between neighboring layers remains constant. This alignment takes place on the initial portion of the curve of magnetization versus magnetic field, on which the slope is large. Under a higher magnetic field the angle θ becomes smaller and the magnetization gradually increases to reach saturation with the external field. When the vectors $\mathbf{M}=(\mathbf{M}_1+\mathbf{M}_2)/2$ are aligned with the external field (Fig. 4b), the magnetizations of neighboring layers are directed at the same angle, $\theta_1=\theta_2=\theta/2$, with respect to the external field. Note that, according to the data of Unguris *et al.*,[7] the initial dimensions of the domains in the iron layers of Fe/Cr superlattices (at zero external field) are $\sim 100\times 100$ μm, i.e.,

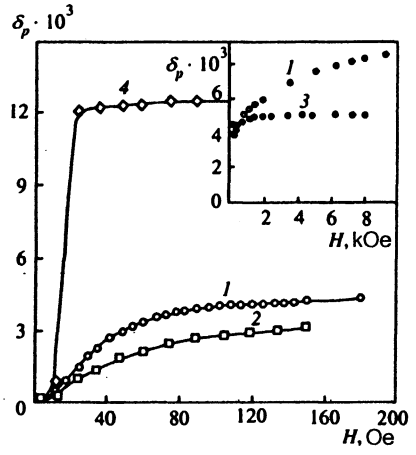

FIG. 5. Intensity of equatorial Kerr effect in Fe/Cr superlattices versus magnetic field: *1)* {Fe(23 Å)/Cr(8 Å)}$_{30}$; *2)* {Fe(20 Å)/Cr(11 Å)}$_{30}$; *3)* {Fe(23 Å)/Cr(27 Å)}$_{12}$; *4)* Fe(d_{Fe}= 1000 Å).

much larger than the wavelength of the light.

The equatorial Kerr effect in a superlattice (Fig. 3b) is described, according to Eqs. (8) and (9), by the equation

$$\delta_p^{(r)} = D_1 \cos \gamma_1 + D_2 \cos \gamma_2, \tag{11}$$

where γ_1 and γ_2 are equatorial magnetization angles of neighboring iron layers. It can be seen in the diagram of Fig. 3b that in a magnetic field perpendicular to the light incidence plane the angles γ_1 and γ_2 in all domains are equal to θ_1 and θ_2: $\gamma_1 = \theta_1 = \gamma_2 = \theta_2 = \theta/2$. The intensities of light reflected from different areas of the reflecting surface should be added, so Eq. (11) for Fe/Cr superlattices takes the form

$$\delta_p^{(r)} = D \cos \frac{\theta}{2}, \tag{12}$$

where $D = D_1 + D_2$ is a function of both diagonal (ϵ_{xx}) and off-diagonal (ϵ_{xz}) components of the dielectric tensors of the superlattice layers, their thicknesses, and the angle of incidence of the light, and θ is the misalignment angle between the magnetic moments of neighboring iron layers, controlled by the external field. The parameter $\mu = \cos(\theta/2)$ is proportional to the specific superlattice magnetization [see Eq. (13) below]. As noted above, in a small magnetic field ($H \ll H_s$)we have $\theta = \theta_0$, where θ_0 is the initial misalignment angle between neighboring layers.

Now let us discuss our measurements. Figure 5 shows the magnetic field dependence of the equatorial Kerr effect for incident light of a wavelength $\lambda = 0.6\mu$m and a angle of incidence $\varphi = 70°$. Independent magnetic measurements demonstrated that "technical saturation" of magnetization is practically achieved in a field of 100–150 Oe. Therefore we assume that at 150 Oe the vectors $\mathbf{M} = (\mathbf{M}_1 + \mathbf{M}_2)/2$ are aligned with the magnetic field (Fig. 4b). The equatorial Kerr effect further increases in a field up to 10 kOe (insert in Fig. 5b) due to the decrease in the angle θ between magnetizations $\mathbf{M}_1$ and $\mathbf{M}_2$. Therefore we measured the initial misalignment angle between $\mathbf{M}_1$ and $\mathbf{M}_2$ using the equatorial Kerr effect in a field $H_0 = 150$ Oe.

Figure 6 shows experimental data on the equatorial Kerr effect versus angle and wavelength taken in a field of 150 Oe in the {Fe(23 Å)/Cr(8 Å)}$_{30}$ supperlattice. Theoretical curves of the effect calculated from Eq. (12) at misalignment angles $\theta_0 = 0°$, 90°, and 126° are also given in Fig. 6. Note that the $\delta_p^{(r)}$-effect calculated at $\theta = 0°$ equals the factor D in Eq. (12). These curves allow us to select optimal conditions for determination of the angle θ_0, given that the amplitude of the $\delta_p^{(r)}$-effect and the factor D peak around $\lambda = 0.6\mu$m and $\varphi = 70°$. In this case the uncertainty of θ_0 is minimized. The initial misalignment angle θ_0 between the iron layers determined at $\lambda = 0.6\mu$m and $\varphi = 70°$ from Eq. (12) is 126°. Its uncertainty calculated at $|\Delta D/D| = 0.1$ is $\Delta\theta_0 = \pm 6°$. The angular and spectral curves of the equatorial Kerr effect calculated at $\theta_0 = 126°$ (solid line in Fig. 6) agree well with the experimental data. The angle θ_0 was derived from measurements at other wavelengths and $\varphi = 70°$, and also at $\lambda = 0.6\mu$m and several angles of incidence. The results are given in Fig. 7. One can see in Fig. 7b that at angles of incidence ranging from 30° to 70° and $\lambda = 0.6\mu$m the calculated angle θ_0 ranges between 126° and 128°, and the angle derived from measurements at $\varphi > 70°$ is smaller because of the poorer accuracy of the $\delta_p^{(r)}$-effect measurements at large angles of incidence. The spread of θ_0 values at different wavelengths is considerably larger (Fig. 7a). In the band of 0.27–0.75 μm we have $\theta_0 \simeq 126°$, but in the IR band this

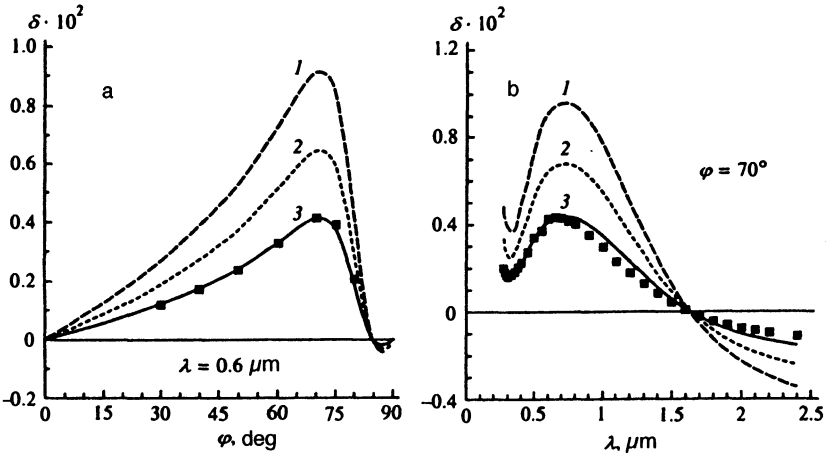

FIG. 6. Intensity of the equatorial Kerr effect versus (a) angle and (b) wavelength in a {Fe(23Å)/Cr(8Å)}$_{30}$ superlattice in a magnetic field $H_0 = 150$ Oe: experimental data are shown by dots, calculations at *(1)* $\theta_0 = 0^0$, *(2)* 90^0, and *(3)* 126^0 are shown as solid lines.

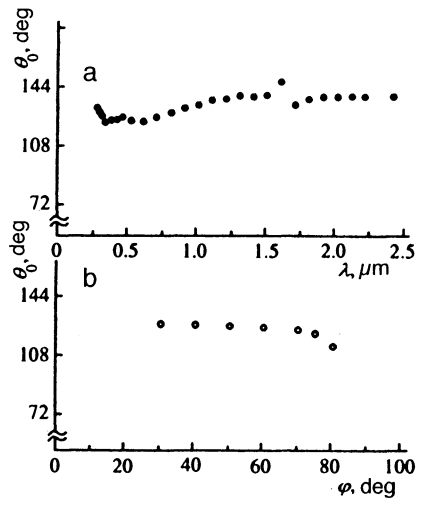

FIG. 7. Measurements of the initial misalignment angle θ_0 versus (a) wavelength and (b) light-incidence angle in the $\{Fe(23\ Å)/Cr(8\ Å)\}_{30}$ superlattice.

angle increases to 140°. The probable cause of this spread of θ_0 at different wavelengths is that in our calculations we used the optical and magneto-optical constants of thick iron and chromium films grown on a substrate from Sitall devitrified glass, and they may be slightly different from those of the iron and chromium epitaxial layers of our superlattices. The angle θ_0 averaged over the measured spectral band is $\langle\theta_0\rangle = 134°$. The relative magnetization $\mu=\cos(\theta/2)$ of sample No. 1 derived from measurements of the $\delta_p^{(r)}$-effect versus magnetic field (Fig. 5b) are plotted in Fig. 8.

The curves of the equatorial Kerr effect versus the wavelength and angle of incidence of the other two superlattices (No. 2 and No. 3) are similar to those given in Fig. 6. They only differ quantitatively in amplitude and are slightly shifted with respect to the points $\lambda=0.6\mu$m and $\varphi=70°$. The initial misalignment angles of these superlattices at $\lambda=0.6\mu$m and $\varphi=70°$ in an external field of 150 Oe are listed in Table I.

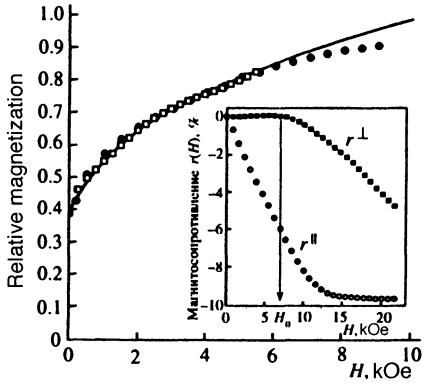

FIG. 8. Relative magnetization $\mu^{\parallel}$ versus magnetic field in the $\{Fe(23\ Å)/Cr(8\ Å)\}_{30}$ superlattice derived from (□) measurements of magnetoresistance and (●) magneto-optical measurements; the solid curve represents the calculations. The insert shows components of the magnetoresistance versus magnetic field.

TABLE I. Angle θ_0 between magnetizations of iron layers in superlattices derived from (a) magneto-optical and (b) magnetoresistance measurements.

No.	Samples	θ_0, deg.	
		a	b
1	$\{Fe(23\ Å)/Cr(8\ Å)\}_{30}$	133	134
2	$\{Fe(20\ Å)/Cr(11\ Å)\}_{30}$	144	147
3	$\{Fe(23\ Å)/Cr(27\ Å)\}_{12}$	80	—

4. MAGNETORESISTANCE OF SUPERLATTICES WITH NONCOLLINEAR ORDERING OF FERROMAGNETIC LAYERS

In this section we discuss a model which describes the magnetoresistance of superlattices with noncollinear ordering of the magnetization in the ferromagnetic layers and demonstrate how the angle between the magnetizations of the layers and the superlattice magnetization curve can be derived from measurements of the magnetoresistance in a magnetic field aligned parallel and perpendicular to the superlattice plane. The underlying principle of this technique was published earlier.[28] The data on the magnetoresistance of the Fe/Cr superlattices will be interpreted in terms of this model.

4.1. Magnetization curves derived from magnetoresistance measurements

Let us consider a superlattice in which the magnetization of ferromagnetic layers separated by layers of a nonmagnetic material alternates between $\mathbf{M}_1$ and $\mathbf{M}_2$. We assume that the absolute values of the vectors $\mathbf{M}_1$ and $\mathbf{M}_2$ are equal and independent of the external magnetic field $\mathbf{H}$:

$$|\mathbf{M}_1|=|\mathbf{M}_2|=M_0.$$

We define the average magnetization of the superlattice, $\mathbf{M}=(\mathbf{M}_1+\mathbf{M}_2)/2$, and the relative magnetizations $\boldsymbol{\mu}_1=\mathbf{M}_1/M_0$, $\boldsymbol{\mu}_2=\mathbf{M}_2/M_0$, and $\boldsymbol{\mu}=\mathbf{M}/M_0$. The absolute value of the relative magnetization $\mu=|\mathbf{M}|/M_0$ is simply related to the angle θ between the vectors $\mathbf{M}_1$ and $\mathbf{M}_2$:

$$\mu=\cos\frac{\theta}{2}. \tag{13}$$

For simplicity, we shall consider only the case which is, in our opinion, most probable in Fe/Cr superlattices, when the magnetization vectors $\mathbf{M}_1$ and $\mathbf{M}_2$ are in the superlattice plane in the ground state ($H=0$).

The shape of the superlattice magnetization curve $\mu(H)$ is controlled by the total effect of the external magnetic field, demagnetization fields, anisotropy field, and effective exchange field. The latter describes the interaction between the magnetizations $\mathbf{M}_1$ and $\mathbf{M}_2$. We denote the energies due to these fields as E_H, E_M, E_A, and E_S and derive the shape of the magnetization curve from the condition that the sum of these energies should be a minimum:

$$E=E_H+E_M+E_A+E_S. \tag{14}$$

The Zeeman energy E_H and the demagnetization energy E_M are

$$E_H=-M_0(\boldsymbol{\mu}\cdot\mathbf{H}), \tag{15}$$

$$E_M = 2\pi M_0^2 \mu_z^2, \tag{16}$$

where μ_z is the projection of the magnetization on the normal to the superlattice plane.

In the anisotropy energy we take into account only the axial anisotropy, assuming that the energy of the in-plane anisotropy is much smaller than the exchange energy:

$$E_A = \frac{1}{2} M_0 H_A \mu_z^2, \tag{17}$$

where H_A is an axial anisotropy field.

As for the interaction between layers, it is reasonable to assume that E_S is a function only of the angle between their relative magnetizations $\boldsymbol{\mu}_1$ and $\boldsymbol{\mu}_2$, i.e., of μ:

$$E_S = M_0^2 J(\mu). \tag{18}$$

The shape of the function $J(\mu)$ in Eq. (18) is not impoprtant as yet. We only assume that this function has a minimum at some $\mu = \mu_0$, $0 < \mu_0 < 1$. The derivative of $J(\mu)$ at $\mu = \mu_0$ is zero: $J'(\mu_0) = 0$.

If the external magnetic field is aligned with the superlattice plane, we have $\mu_z = 0$, $E_M = E_A = 0$, and the condition of minimum energy, $\partial E/\partial \mu = 0$, yields the following equation for the curve of "parallel" magnetization $\mu^{\parallel}(H)$:

$$M_0 J'(\mu^{\parallel}) = H, \quad H \leqslant H_S^{\parallel}, \tag{19}$$

where $H_S^{\parallel} = M_0 J'(1)$ is the saturation field of the parallel magnetization.

Equation (19) may be considered as a definition of the field $H^{\parallel}(\mu)$ at which the magnetization $\mu^{\parallel}$ equals the given value μ:

$$H^{\parallel} = M_0 J'(\mu), \quad \mu_0 \leqslant \mu \leqslant 1. \tag{20}$$

If the field **H** is perpendicular to the superlattice plane, the curve of the perpendicular magnetization $\mu^{\perp}(H)$ is derived from the conditions of minimum energy, $\partial E/\partial \mu = 0$ and $\partial E/\partial \mu_z = 0$. For $H \leqslant H_0 = (4\pi M_0 + H_A)\mu_0$ the absolute value of the magnetization $\mu^{\perp}(H)$ is independent of H and equals μ_0, and its z-component $\mu_z^{\perp}(H)$ is linear in H:

$$\mu^{\perp}(H) \equiv \mu_0, \quad \mu_z^{\perp}(H) = H/H_0, \quad H \leqslant H_0. \tag{21}$$

For $H_0 \leqslant H \leqslant H_S^{\perp}$, where $H_S^{\perp} = H_S^{\parallel} + 4\pi M_0 + H_A$ is the saturation field of the perpendicular magnetization, the parameters $\mu^{\perp}(H)$ and $\mu_z^{\perp}(H)$ are equal and are determined by the equation

$$M_0 J'(\mu^{\perp}) + \frac{H_0}{\mu_0}\mu^{\perp} = H. \tag{22}$$

Equation (22) may be considered as a definition of the field $H^{\perp}(\mu)$, at which the magnetization $\mu^{\perp}$ equals the given value $\mu \geqslant \mu_0$:

$$H^{\perp} = M_0 J'(\mu) + \frac{H_0}{\mu_0}\mu. \tag{23}$$

A relation among $H^{\perp}$, $H^{\parallel}$, and μ can be easily derived from Eqs. (20) and (23):

$$\frac{H^{\perp}(\mu) - H^{\parallel}(\mu)}{H^{\perp}(\mu_0)} = \frac{\mu}{\mu_0}. \tag{24}$$

In order to include the magnetoresistance, we assume that at any orientation of the magnetic field the superlattice resistance $R(\mathbf{H})$ depends on **H** only through the effect of the magnetic field on the misalignment angle between neighboring layers. In fact, this assumption means that $R(\mathbf{H})$ is a function of $\mu(\mathbf{H})$:

$$R(\mathbf{H}) = F(\mu(\mathbf{H})). \tag{25}$$

Let us define the relative magnetoresistance $r(\mathbf{H}) = [R(\mathbf{H}) - R(0)]/R(0)$. The quantity $r^{\parallel}(H)$ denotes the magnetoresistance when the field **H** is parallel to the current density parallel to the superlattice plane and is called longitudinal. The magnetoresistance in the field perpendicular to the layers is called perpendicular and denoted as $r^{\perp}(H)$. Then the following relations can be derived from Eq. (25):

$$r^{\parallel}(H) = \frac{F(\mu^{\parallel}(H)) - F(\mu_0)}{F(\mu_0)}, \tag{26}$$

$$r^{\perp}(H) = \frac{F(\mu^{\perp}(H)) - F(\mu_0)}{F(\mu_0)}. \tag{27}$$

An important feature of the perpendicular magnetoresistance of superlattices with noncollinear magnetic ordering ($\mu_0 \neq 0$) can be derived from Eq. (27). If the magnetic field ranges between 0 and H_0, $\mu^{\perp}(H)$ in our model is independent of H and equals μ_0. Hence the perpendicular magnetoresistance in this range should be zero. Viewing the experimental curve of $r^{\perp}(H)$ measured in {Fe(23 Å)/Cr(8 Å)}$_{30}$ (insert in Fig. 8) in light of this, one can easily see that $r^{\perp}(H)$ is practically constant in a fairly wide range of magnetic fields, and at higher fields it is negative. In our opinion, this fact is a direct indication that magnetizations of neighboring iron layers are not collinear in the initial state.

Using Eqs. (26) and (27), we can easily derive the ratio $\eta(H) = \mu^{\parallel}(H)/\mu_0$ as a function of the field from measurements of $r^{\perp}(H)$ and $r^{\parallel}(H)$. The function $\eta(H)$ has the form

$$\eta(H) = \frac{H^{\perp}(r^{\parallel}(H)) - H}{H^{\perp}(0)}, \tag{28}$$

where $H^{\perp}(r)$ is the magnetic field at which the perpendicular magnetoresistance equals a given value r.

The numerical value of μ_0 can be also derived from measurements of $\eta(H) = \mu^{\parallel}(H)/\mu_0$. This procedure, however, demands an explicit expression for the exchange energy $J(\mu)$.

4.2. Model of biquadratic exchange

Suppose that the energy of exchange between magnetic layers can be expanded in powers of $\boldsymbol{\mu}_1 \cdot \boldsymbol{\mu}_2$. Taking only the first two terms of this expansion, we present E_S as[29]

$$E_S = M_0^2 J_1 (\boldsymbol{\mu}_1 \cdot \boldsymbol{\mu}_2) + M_0^2 J_2 (\boldsymbol{\mu}_1 \cdot \boldsymbol{\mu}_2)^2, \tag{29}$$

where J_1 and J_2 are constants. The first term on the right of Eq. (29) is called bilinear, and the second term biquadratic. The bilinear interaction leads to ferromagnetic ordering for $J_1 < 0$ and $J_2 = 0$, and to antiferromagnetic ordering for $J_1 > 0$ and $J_2 = 0$. The biquadratic interaction (at $J_1 = 0$) leads to a magnetic order with perpendicular magnetizations

$\mathbf{M}_1$ and $\mathbf{M}_2$. The sum of the two terms in Eq. (29) leads to the noncollinear alignment with an arbitrary angle θ_0 between $\mathbf{M}_1$ and $\mathbf{M}_2$.

From $(\boldsymbol{\mu}_1 \cdot \boldsymbol{\mu}_2) = 2\mu^2 - 1$, the function $J(\mu)$ in the definition of E_S [Eq. (18)] can be expressed as

$$J(\mu) = -J_1 + J_2 + 2[J_1 - 2J_2(1-\mu^2)]\mu^2. \tag{30}$$

The equilibrium magnetization μ_0 at given J_1 and J_2 can be derived from the condition of minimum $E_S(\mu)$ on the interval $0 \leqslant \mu \leqslant 1$. The plane defined by the coordinates (J_1, J_2) can be separated into three regions. In the first region, $J_1 > 0$, $J_2 < J_1/2$, the magnetization satisfies $\mu_0 \equiv 0$, which means antiferromagnetic ordering. In the second region, $J_1 < 0$, $J_2 < -J_1/2$, the magnetization satisfies $\mu_0 \equiv 1$, which means ferromagnetic ordering. In the third region defined by the relation $J_2 > |J_1|/2$ the magnetic ordering is noncollinear and the relative magnetization is

$$\mu_0 = \left(\frac{1}{2} - \frac{J_1}{4J_2}\right). \tag{31}$$

Below we shall discuss magnetization curves typical of the third region.

Equation (19) can be transformed with due account of Eqs. (30) and (31) to

$$\frac{\mu^{\parallel}(H)[(\mu^{\parallel}(H))^2 - \mu_0^2]}{1-\mu_0^2} = \frac{H}{H_S^{\parallel}}, \tag{32}$$

where

$$H_S^{\parallel} = 4(J_1 + 2J_2)M_0. \tag{33}$$

In what follows we shall consider only the parameters μ_0 and $H_S^{\parallel}$, since they uniquely define J_1 and J_2 by virtue of Eqs. (31) and (33). The solution of Eq. (32) can be expressed as

$$\mu^{\parallel}(H) = \mu_0 \eta_h(H), \tag{34}$$

where

$$\eta_h(H) = \left[\frac{H}{h} + \frac{1}{3}\sqrt{\left(3\frac{H}{h}\right)^2 - \frac{1}{3}}\right]^{1/3} + \left[\frac{H}{h} - \frac{1}{3}\sqrt{\left(3\frac{H}{h}\right)^2 - \frac{1}{3}}\right]^{1/3}. \tag{35}$$

The parameter in the function of Eq. (35) is

$$h = \frac{2\mu_0^3}{1-\mu_0^2} H_S^{\parallel}, \tag{36}$$

and it determines the shape of the curve $\mu^{\parallel}(H)/\mu_0$.

Now let us use the function $\eta_h(H)$ defined by Eq. (35) to approximate the experimental curve $\eta(H)$ derived from measurements of the magnetoresistance. The parameter h will be varied in order to minimize the RMS deviation of the curve $\eta_h(H)$ from $\eta(H)$:

$$\Delta\eta(h) = \frac{\int_0^{H_m}[\eta_h(H) - \eta(H)]^2 dH}{\int_0^{H_m}\eta^2(H)dH}, \tag{37}$$

where H_m is the upper boundary of the interval on which the function $\eta(H)$ has been measured. The curve of $\eta_h(H)$ is best fitted to $\eta(H)$ at $h = h_0$ determined by the condition

$$\frac{d}{dh}\Delta\eta(h) = 0. \tag{38}$$

The relative RMS error of the approximation is $\Delta\eta_0 = \Delta\eta(h_0)$.

Having found the parameter h in this way and having derived the saturation field $H_S^{\parallel}$ from measurements of $r^{\parallel}(H)$, we can determine μ_0 of a given superlattice using Eq. (36).

Since $H_S^{\parallel}$ cannot be determined unambiguously from the curve of $r^{\parallel}(H)$, we define $H_S^{\parallel}$ as the field at which $r^{\parallel}(H) = 0.85 r_m^{\parallel}$ holds, where $r_m^{\parallel}$ is the maximum longitudinal magnetoresistance measured in our experiments.

The curves of the magnetoresistance versus magnetic field of the {Fe(23 Å)/Cr(8 Å)}$_{30}$ superlattice are given in the insert of Fig. 8. The saturation field derived from these curves $H_S^{\parallel} \simeq 10.1$ kOe. The solution of Eqs. (38) and (36) yields the relative magnetization $\mu_0 = 0.387$. This parameter corresponds to a misalignment angle $\theta_0 = 134°$. The RMS deviation of the calculated curve from experimental data is reasonably small, which indicates that the theoretical curve is close to the experimental one.

Thus we have determined both μ_0 and h in Eq. (34) for $\mu^{\parallel}(H)$. The solid curve in Fig. 8 is a calculation of the relative magnetization $\mu^{\parallel}$ versus magnetic field by Eqs. (34) and (35) using μ_0 and h derived from the least-square fitting. The function $\mu^{\parallel}(H) = \mu_0 \eta(H)$ derived from experimental data on $r^{\perp}(H)$ and $r^{\parallel}(H)$ using Eq. (28) for $\eta(H)$ is indicated by open squares. The relative magnetization derived from magneto-optical measurements is shown by full circles.

The angle between the magnetization vectors of neighboring iron layers in the superlattice with 20-Å iron and 11-Å chromium layers derived from our experimental data at zero magnetic field is $\theta_0 = 147°$.

Thus the two techniques proposed in this paper yield close values of θ_0 (Table I) and similar curves of $\mu^{\parallel}(H)$.

CONCLUSION

We have proposed two techniques for independent determination of the magnetic order in metal superlattices. One of them uses the equatorial Kerr effect, the other the effects of magnetic ordering on magnetoresistance. Measurements of the initial misalignment angle θ_0 between neighboring iron layers and of the relative magnetization ($\mu = \cos(\theta/2)$) versus magnetic field using both techniques have yielded similar results. We found that in the superlattices studied the magnetic ordering is noncollinear with a misalignment angle between iron layers ranging from 80° to 147°.

The work was supported by the Russian Fund for Fundamental Research (project No. 93-02-15104) and International Science Foundation (grant NMK000).

[1] S. Haschimoto and Y. Ochiai, J. Magn. Magn. Mat. **88**, 211 (1990).
[2] D. Weller, W. Reim, and K. Spörl, J. Magn. Magn. Mat. **93**, 183 (1991).
[3] Yu. V. Kudryavtsev and R. Gontazh, Fizika Metallov i Metallovedenie **77** (6), 44 (1994).

[4]P. Grünberg, R. Schreiber, Y. Pang *et al.*, Phys. Rev. Lett. **57**, 2442 (1986).
[5]M. N. Baibich, J. M. Broto, A. Fert *et al.*, Phys. Rev. Lett. **61**, 2472 (1988).
[6]S. S. P. Parkin, N. More, and K. P. Roche, Phys. Rev. Lett. **64**, 2304 (1990).
[7]J. Unguris, R. J. Celotta, and D. T. Pierce, Phys. Rev. Lett. **67**, 140 (1991).
[8]E. E. Fullerton, M. J. Conover, J. E. Mattson *et al.*, J. Appl. Phys. **75**, 6461 (1994).
[9]P. Bruno and C. Chappert, Phys. Rev. B **46**, 261 (1992).
[10]M. van Schilfgaarde and W. A. Harrison, Phys. Rev. Lett. **71**, 3870 (1993).
[11]H. Nukanishi, T. Tamuro, H. Kasai, and A. Okiji, J. Magn. Magn. Mat. **126**, 394 (1993).
[12]S. S. Parkin, A. Mansour, and G. P. Felcher, Appl. Phys. Lett. **58**, 1479 (1991).
[13]P. Grünberg, J. Barnes, F. Saurenbach *et al.*, J. Magn. Magn. Mat. **93**, 58 (1991).
[14]S. Demokritov, J. A. Wolf, and P. Grünberg, Europhys. Lett. **15**, 881 (1991).
[15]N. Hosoito, K. Mibu, T. Ono *et al.*, J. Magn. Magn. Mat. **126**, 255 (1993).
[16]C. D. Potter, R. Schad, P. Beliën *et al.*, Phys. Rev. B **49**, 16055 (1994).
[17]A. Schrever, J. F. Ankner, M. Schäfer *et al.*, *14-th Intern. Colloquium on Magnetic Films and Surfaces*, Colloquium Digest, B137 (1994).
[18]G. A. Bolotin, M. M. Kirillova, L. V. Nomerovannaya *et al.*, Fizika Metallov i Metallovedenie **78**, 57 (1994).
[19]I. D. Lobov, A. V. Druzhinin, S. L. Veremeenko, and A. A. Makhnev, Manuscript deposited at VINITI, No. 2324, Novosibirsk (1988).
[20]A. V. Rzhanov, K. K. Svitashev, A. S. Merdezhov, and V. A. Shvets, Dokl. Akad. Nauk SSSR **298**, 862 (1988).
[21]A. B. Shaikin, M. M. Kirillova, N. V. Minulina, and A. N. Rakitshiĭ, Fizika Metallov i Metallovedenie **66**, 695 (1988).
[22]V. P. Shirokovskiĭ, M. M. Kirillova, and N. A. Shilkova, Zh. Éksp. Teor. Fiz. **82**, 784 (1982)[Sov. Phys. JETP **55**, 404 (1982)].
[23]P. G. Guletskiĭ, Yu. V. Knyazev, M. M. Kirillova, and L. M. Sandratskiĭ, Fizika Metallov i Metallovedenie **67**, 279 (1989).
[24]G. A. Bolotin and V. M. Maevskiĭ, Fizika Metallov i Metallovedenie **79** (5), 8 (1995).
[25]O. Heavens, *Optical Properties of Solids*, Butterworth, London (1955), p. 155.
[26]V. M. Maevskiĭ, Manuscript deposited at VINITI No. 2461-B93, Moscow (1993).
[27]W. Folkerts, J. Magn. Magn. Mater. **94**, 302 (1991).
[28]V. V. Ustinov, V. I. Minin, L. N. Romashev *et al.*, Fizika Metallov i Metallovedenie **8** (2) (1995).
[29]M. Rührig, R. Schäfer, A. Hubert *et al.*, Phys. Status Sol. (a) **125**, 635 (1991).

Translation provided by the Russian Editorial office.